Analysis of Line Distance Elements for Various IBR Controllers and System Conditions

Paulo Henrique Pinheiro, Bruno W. França, Yona Lopes, Soham Chakraborty, Rômulo G. Bainy, Hangtian Lei, Brian K. Johnson, Scott Manson, Jing Wang, Rasel Mahmud, Andy Hoke and Cameron J. Kruse

***Abstract*—The large-scale penetration of inverter-based resources in power systems has challenged protection engineers because of the different fault behaviors these sources provide compared to conventional generation systems. The main challenges include a low level of fault current magnitude, unpredictable angles of sequence currents, and lack of inertia that can lead to maloperation of conventional phasor-based protection elements. This paper presents a sensitivity analysis of transmission line distance protection elements during phase-to-ground and phase-to-phase faults for different inverter controllers and power system conditions. It also summarizes which line protection elements remain secure near IBR terminations and identifies the ones affected by the inverter-based response. The paper concludes by highlighting that regulating negative-sequence current injection during the fault aids correct protection decisions, but does not address the entire challenge. Finally, alternative protection elements to those affected by the inverter fault response are discussed.**

***Keywords*—Transmission Lines, Distance Protection, Inverter-Based Resources, Grid Following Inverters.**

I. Introduction

THE large-scale penetration of Inverter-Based Resources (IBRs) in power grids challenges protection engineers to apply secure and dependable protection schemes because conventional protection algorithms were developed assuming conventional sources like a Synchronous Generators (SG). In conventional power systems, the fault behavior is predictable, thus enabling the use of reliable polarizing quantities for protection elements. Recent publications regarding protecting power systems with increased penetration of IBRs lists the following items as current challenges [1], [2], [3], [4]: incorrect operation in memory polarized distance elements due to fast frequency excursion; negative-sequence-based protection elements failure to pick up due to lack of negative-sequence current and/or malfunction due to unconventional negative-sequence current angle; Fault-Type Identification (FID) logic based on sequence currents may fail to correctly identify the fault type due to unconventional angle of sequence currents; and distance protection elements failure to pick up because the supervision logic is not fulfilled.

Solutions designed to overcome these challenges are mainly focused on developing protection algorithms agnostic to source nature feeding the fault [5], [6]. Other approaches focus on time-domain distance and directional elements by applying super-imposed quantities, thus isolating the pure fault circuit [7]. Travelling wave-based methods also offer an outlet for protecting lines fed by IBRs because of their fast response when compared to IBR controllers [8]. Additionally, time-domain distance protection based on super-imposed quantities specially developed for lines interconnecting inverter-based sources can also be used [9].

On the source side, the IEEE Std. 2800-2022 [10] provides requirements for current injection for IBRs to make their fault response more predictable. IEEE 2800-compliant inverters benefit conventional phasor-based protection algorithms because they enable consistent sequence network response. Recent publications investigated this topic with promising conclusions. In [11], the authors discuss the improvements enabled in phasor and incremental quantities-based fault selection logic when the IBR regulates negative-sequence current injection during faults. In [12], the authors evaluate the behavior of various protection functions (i.e., distance, differential, directional elements, and FID logic based on sequence currents) to different IBRs outer-loop and inner-loop controller options. The main takeaway from these studies is that negative-sequence regulation can improve the reliability of phasor-based protection functions.

This paper is an extension of [4] and [12]. Our previous work aimed to determine which IBR modeling aspects impact the inverter fault response and their subsequent effects on protection functions. [4] gives a perspective from the IBR side, whereas [12] focus more on the protection function point of view. In this work, we focus on evaluating combinations of protection elements for an enhanced protection scheme design for lines interfacing

This work was authored by the National Renewable Energy Laboratory (NREL), operated by Alliance for Sustainable Energy, LLC, for the U.S. Department of Energy (DOE) under Contract No. DE-AC36-08G*O*28308. Funding provided by U.S. Department of Energy Office of Energy Efficiency and Renewable Energy Solar Energy Technologies Office. The views expressed in the article do not necessarily represent the views of the DOE or the U.S. Government. The U.S. Government retains and the publisher, by accepting the article for publication, acknowledges that the U.S. Government retains a nonexclusive, paid-up, irrevocable, worldwide license to publish or reproduce the published form of this work, or allow others to do so, for U.S. Government purposes. This work is also supported by Coordenação de Aperfeiçoamento de Pessoal de Nível Superior - CAPES under grant 001.

Paulo Henrique Pinheiro, Bruno W. França, and Yona Lopes are with the Fluminense Federal University, Niterói, RJ 24210-240 BR (e-mail of corresponding author: paulopinheiro@id.uff.br)

Rômulo Gonçalves Bainy, Hangtian Lei, and Brian K. Johnson are with the University of Idaho, Moscow, ID 83843 USA.

Soham Chakraborty, Jing Wang, Rasel Mahmud and Andy Hoke are with the National Renewable Energy Laboratory, Golden, CO 80401 USA.

Scott Manson is with the Schweitzer Engineering Laboratories, Pullman, WA 99163 USA.

Cameron J. Cruise is with Kauai Island Cooperative Utility, Lihue, HI 96766 USA.

Paper submitted to the International Conference on Power Systems Transients (IPST2025) in Guadalajara, Mexico, June 8-12, 2025.

inverters. The contributions are: 1) the analysis of three sets combining different distance protection elements with different supervising functions for a performance comparison; 2) the investigation of fault resistance effects in the distance elements, highlighting the behavior of quadrilateral characteristic with negative-sequence current polarization; 3) observations regarding system nonhomogeneity and how it is impacted by IBRs; 4) details on the behavior of the FID logic regarding its operation alongside supervising elements; 5) insights regarding the supervision of impedance-based directional elements and the impacts in their operation; and 6) effects of IBR current limiter priority during fault over the resistive reach of mho phase elements. The outline of the paper begins with Section II where we describe the power system under study. Section III presents the modeling of the protection elements evaluated in this paper. Section IV discusses the case studies and results, and finally Section V presents the conclusions.

II. Power System Under Study

Figure 1 presents the 57.1 kV power system under study simulated in PSCAD/EMTDC. This system is based on an existing transmission network in the United States. The equivalent power system is connected to bus 1 through line 1. The equivalent grid is in parallel to a 6.9 kV 7.5 MVA hydro turbine generator connected to the bus via a 57.1/6.9 kV 7.5 MVA Dyn1 power transformer. The line of interest for the studies is line 2. R1 and R2 represent the relays protecting the line. Bus 2 connects the 480 V 14 MVA IBR system to the grid through a 57.1/0.48 kV 14 MVA Dyn1 power transformer. The transformer TF2 connection is originally Dyn1. However, to study the behavior of ground faults in this system, the connection was changed to YNd1 to allow zero-sequence current circulation behind relay R2. Table I presents the IBR model parameters.

This work evaluates the protection response for the inverter operating in Grid Following (GFL) mode. The primary DC source is a Photovoltaic (PV) combined with a Battery Energy Storage System (BESS). Table II lists the control options for the GFL inverter. The inverter can have its outer-loop controller set as either PQ dispatch or Vdc-Vac control. The inner-loop current controller controls phase currents using either dq or $\alpha\beta$ reference frames [13]. In addition, the simulated IBR can regulate positive and negative sequence currents in the dq frame in compliance with IEEE Std. 2800-2022 [10]. The different control options are varied systematically using the Python automation library available in PSCAD/EMTDC through the framework described in [4]. The IBRs controllers include current limiting logic consistent with industry practices [1], [14]. The available options for the current limiting logic is saturation or latching types. Prioritization can be set to either q-axis or d-axis components for phase and sequence inner-loop current controllers. And α-axis or β-axis priority for $\alpha\beta$-domain controllers.

III. Protection Relay Modelling

The transmission system under study is protected by a line-differential scheme (87L) and distance elements. The analysis for the 87L presented in [12] proved the scheme's reliability, so this paper focuses only on the distance elements and their supervising functions, such as directional elements. The protection algorithms are developed using Matlab. The algorithm reads COMTRADE files from PSCAD and outputs the protection response of each element according to the simulated scenario. The distance characteristics are described in Sections III-A and III-B. The directional elements are described in Section III-C, and the FID logic in Section III-D. The response of these protection elements against faults fed by IBRs provides the basis for investigating how different controls affect the relay response.

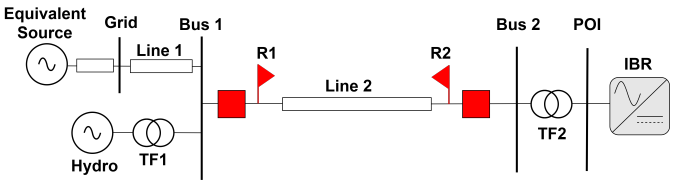

Fig. 1: Power system under study.

TABLE I: EMT model parameters for the IBR.

Inverter Parameters	Values
Ratings (3ϕ)	480 V, 60 Hz, 14 MVA
DC side	Vdc = 1200 V, fs = 5 kHz
LCL filter	Lf = 15 uH, Lg = 1.5 uH, Cf = 280 uF

TABLE II: Control options for GFL operating mode.

Controller Type		
Outer Power Control		Inner Current Control
Active Power	Reactive Power	
Open-loop P dispatch	Open-loop Q dispatch	Phase currents in dq-domain
Closed-loop P dispatch	Closed-loop Q dispatch	Phase currents in ab-domain
Vdc control	Vac control	Sequence currents in dq-domain

A. Memory Polarized Mho Distance Element

Figure 2 presents the positive-sequence memory polarized mho element. The filter used for memory polarization is presented in (1) [15]. $V_{1,mem}$ is the positive sequence voltage with memory, V_1 is the positive sequence voltage, α is a weighting factor that selects the amount of memory voltage to be implemented, in our study $\alpha = 1/16$ [16]. k is the actual sample of the variables. The "m" equation, shown in (2), is used to compute the distance to the fault. $1\angle Z_{1L}$ is the transmission line positive-sequence angle. Table III expands the V and I terms for two fault loops studied in this work (i.e., AG, and BC). The memory voltage, $V_{1,mem}$, is also listed.

$$V_{1,mem(k)} = \alpha \cdot V_{1(k)} - (1-\alpha) \cdot V_{1,mem(k-halfcycle)} \quad (1)$$

$$m = \frac{Re[V \cdot V^*_{1,mem}]}{Re[1\angle Z_{1L} \cdot I \cdot V^*_{1,mem}]} \ (\Omega) \quad (2)$$

TABLE III: Mho element operating and polarizing quantities

Fault Loop	V	I	$V_{1,mem}$
AG	V_A	$I_A + k_0 \cdot I_R$	$V_{A1,mem}$
BC	$V_B - V_C$	$I_B - I_C$	$V_{BC,1mem}$

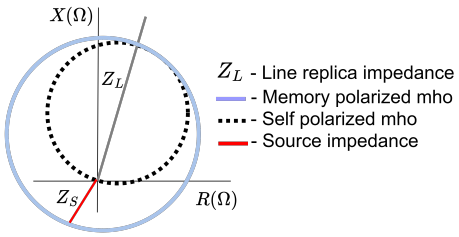

Fig. 2: Memory polarized mho element.

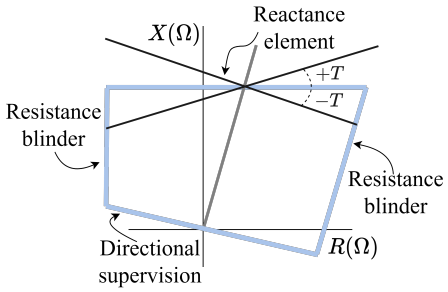

Fig. 3: Quadrilateral characteristic.

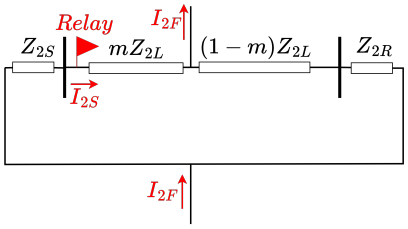

Fig. 4: Negative-sequence network.

This approach is available in commercial relays [17], and it achieves economy in computer processing by mapping the points of a mho circle onto a unique point in a line equivalent to the zone reach [18].

B. Quadrilateral Characteristic

The quadrilateral characteristic, shown in Figure 3, uses four comparators to detect a fault: the reactance element, the fault resistance blinders, and directional supervision. The reactance element uses (3) to estimate the fault distance from the relay location for ground and phase faults [19]. The V and I terms are the same as for the mho element.

$$X = \frac{Im[V \cdot (I_{POL} \cdot 1\angle T)^*]}{Im[1\angle Z_{1L} \cdot I \cdot (I_{POL} \cdot 1\angle T)^*]} \ (\Omega) \tag{3}$$

I_{POL} is the polarizing current for the reactance element. It can be either I_2 or I_0 for ground faults, and I_2 for phase faults. These currents are used because they better approximate the total fault current angle. The tilting angle T compensates for the effects of nonhomogeneous power systems. It is computed using (4) for negative-sequence current polarization, following the sequence network diagram shown in Figure 4 [20]. This angle computes the phase shift between the polarizing and the total fault current. Therefore, the effects of fault resistance in systems with remote infeed are effectively removed from the reactance element [21]. A similar analysis applies to the zero-sequence current polarization.

$$T = arg\left[\frac{Z_{2S} + Z_{2L} + Z_{2R}}{(1-m) \cdot Z_{2L} + Z_{2R}}\right] \ (^\circ) \tag{4}$$

The fault resistance for phase-to-ground faults is estimated using (5) [22]. For phase-to-phase faults, the relay uses (6) [19].

$$Rf = \frac{Im[V_\phi \cdot (1\angle Z_{1L} \cdot (I_\phi + k_0 \cdot I_R))^*]}{Im[\frac{3}{2}(I_2 + I_0)(1\angle Z_{1L} \cdot (I_\phi + k_0 \cdot I_R))^*]} \ (\Omega) \tag{5}$$

$$Rf = \frac{Im[V_{\phi\phi} \cdot (1\angle Z_{1L} \cdot (I_{\phi\phi}))^*]}{Im[(j \cdot 2\sqrt{3} \cdot I_2) \cdot (1\angle Z_{1L} \cdot (I_{\phi\phi}))^*]} \ (\Omega) \tag{6}$$

C. Directional Elements

This work evaluates the zero-sequence (32V) and negative-sequence (32Q and 32QG) voltage polarized directional elements. The 32V and 32QG elements supervise the ground distance elements, and the 32Q supervises phase distance elements. The zero-sequence directional element uses (7) to estimate the effective equivalent impedance the relay sees. The negative-sequence directional element uses (8) [23].

$$z0 = \frac{Re[3V_0 \cdot (3I_0 \cdot 1\angle Z_{0L})^*]}{|3I_0|^2} \ (\Omega) \tag{7}$$

$$z2 = \frac{Re[V_2 \cdot (I_2 \cdot 1\angle Z_{1L})^*]}{|I_2|^2} \ (\Omega) \tag{8}$$

The estimated impedances are compared against forward and reverse dynamic thresholds to determine fault direction. For instance, if z2 < Z2FTH, the 32Q or 32QG elements declare a forward fault. If z2 > Z2RTH, the element declares a reverse fault. A similar analysis applies to the 32V element. Z2FTH is computed using (9), and Z2RTH is computed using (10) [17]. $Z2F$ and $Z2R$ are coefficients set in the relay for forward and reverse faults, respectively.

$$\begin{cases} Z2FTH = 0.75 \cdot Z2F - \left(0.25 \cdot \left|\frac{V2}{I2}\right|\right) \ if \ Z2F \leq 0 \\ Z2FTH = 1.25 \cdot Z2F - \left(0.25 \cdot \left|\frac{V2}{I2}\right|\right) \ if \ Z2F > 0 \end{cases} \tag{9}$$

$$\begin{cases} Z2RTH = 0.75 \cdot Z2R + \left(0.25 \cdot \left|\frac{V2}{I2}\right|\right) \ if \ Z2R \geq 0 \\ Z2RTH = 1.25 \cdot Z2R + \left(0.25 \cdot \left|\frac{V2}{I2}\right|\right) \ if \ Z2R < 0 \end{cases} \tag{10}$$

D. Fault-Identification Logic

The FID logic monitors the angle difference between the negative and zero-sequence current in the phase A reference frame [24]. It compares three separate regions, each of 60 degrees, to classify the phases involved in phase-to-ground and double-line-to-ground faults, as shown in Figure 5. Once the faulted phases have been identified, the logic selects

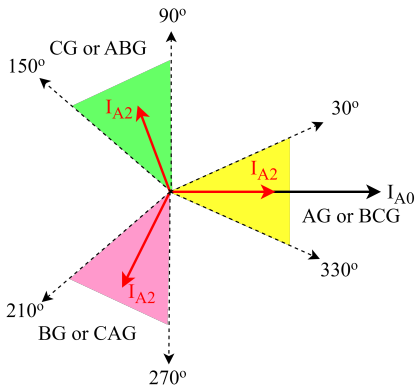

Fig. 5: FID logic.

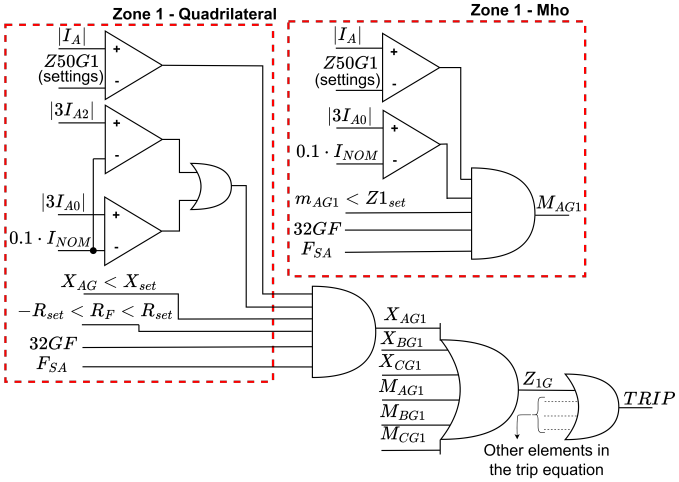

Fig. 6: Zone 1 schematic diagram for AG faults.

the fault loop with the smaller estimated reach using the mho element to differentiate between double-line-to-ground and single-line-to-ground faults. For example, the fault loop centered on 0 degrees can either be an AG or BCG fault. if the AG fault loop shows a smaller effective reach, the fault is identified as AG. If the BC loop has a smaller effective impedance, the fault is identified as BCG. This, in turn, determines the distance element to enable.

E. Zone 1 schematic diagram

Figure 6 presents a diagram for the zone 1 element for AG faults using the quadrilateral and the mho characteristics. A similar diagram applies to other fault loops and zone 2 elements. The operation criteria for the quadrilateral element are: the estimated reactance, X_{AG}, needs to be below its threshold, and the estimated fault resistance R_F needs to be between the resistive blinders (i.e., $-R_{set} < R_F < R_{set}$). The directional element declares forward fault by asserting the 32GF bit using either the 32V or 32QG elements, and the FID logic enables the AG loop to operate using $F_{SA} = 1$. Similarly, the mho element compares the fault reach estimation with the zone 1 threshold (i.e., $mAG1 < Z1_{set}$).

IV. Case Studies and Results

In [12], the response of mho distance elements to ground faults is not impacted by different types of current controllers from the IBRs. The elements that rely on the negative-sequence current (i.e., reactance element for ground and phase faults, 32Q directional element, and FID logic) can be used reliably only if the IBR regulates negative-sequence current injection in compliance with IEEE Std. 2800-2022 [10] or a similar requirement stipulating magnitude and angle ranges for the negative sequence current. Despite these promising conclusions, the cases presented in that work considered only bolted faults. This work considers additional cases not covered in [12] to extend the analysis on the limitations of distance elements when protecting lines supplied by IBRs. Table IV describes the evaluated scenarios, resulting in a total of 198 cases.

A. Effects of resistive faults seen by distance elements

The case study considers phase-A-to-ground faults with fault resistance values ranging from 0 to 10 Ω in steps of 1 Ω with the following fault locations: 5, 50, and 80 % of the line relative to Bus 2. Table V presents three different combinations of protection elements for the analysis.

From the total of 198 cases, 67% of the cases did not result in a relay operation because of lacking negative-sequence current supplied by the inverter. Effectively, the relay could detect faults in the remaining 33 % of the cases, where the inverter regulates positive and negative-sequence currents. Figure 7 presents a performance comparison of the quadrilateral and mho distance elements for these remaining cases considering the set combinations presented in Table V. XAG1 and XAG2 represent the quadrilateral element using zone 1 and zone 2, and MAG1 and MAG2 represent the mho element using zone 1 and zone 2. In these results, correct operations refer to the zone 1 or zone 2 pickup for faults within the protection zone.

TABLE IV: Simulated conditions

TF2 connection	YNd1 (YN winding facing the system)
Power-flow (p.u.)	P = 0.25, Q = 0.0.
Power-control	PQ dispatch
Inner current control	1 - phase currents in dq-domain 2 - phase currents in $\alpha\beta$ domain 3 - sequence currents in dq-domain
Current limiting logic	1 - Saturation q axis 2 - Saturation ($\alpha\beta$)
Faut location (p.u.)	1 - 0.05 2 - 0.5 3 - 0.8
Fault resistance (Ω)	0 to 10 in steps of 1
Hydro operation	1 - on 2 - off

TABLE V: Protection Elements Combination.

Protection Functions	**Set 1**	**Set 2**	**Set 3**
Distance Element	1 - I0 polarized quad element 2 - V1mem polarized mho	1 - I2 polarized quad element 2 - V1mem polarized mho	1 - I2 polarized quad element 2 - V1mem polarized mho
Directional Supervision	1 - 32V element	1 - 32QG element	1 - 32V element
FID logic	1 - Sequence currents-based FID		

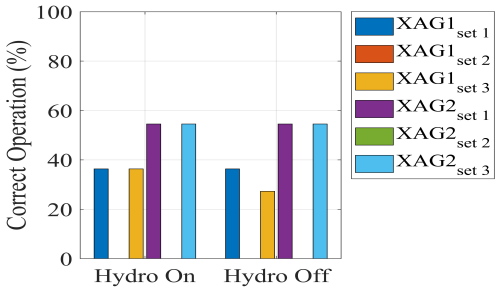

(a) Quadrilateral element.

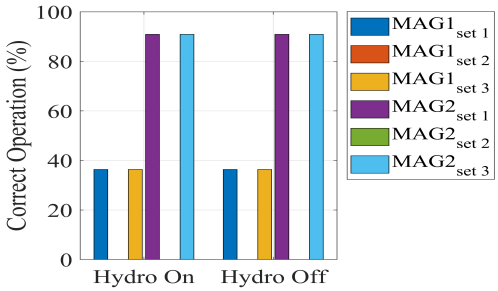

(b) Mho element.

Fig. 7: Percentage of correct quadrilateral and mho element responses during resistive faults - set 2 gives 0%.

The following conclusions can be drawn: considering the three sets of elements available in Table V, zone 1 of distance protection for both mho and quadrilateral elements could cover a similar number of cases. The quadrilateral characteristic with I_2 polarization resulted in fewer operations when the hydro plant was offline. The mho element covered more fault resistance than the quadrilateral element in zone 2, and the distance elements did not operate when they were supervised by the 32QG directional element (i.e., set 2 in Table V), this is explained in Section IV-D. Further explanation is provided in the next sections.

B. Distance Elements

The quadrilateral characteristic operation is influenced by its polarizing current. This element has a more reliable behavior using zero-sequence current polarization. Notice in Figure 7a that $XAG1_{set1}$ operate for the same amount of cases considering the Hydro plant on or off, whereas $XAG1_{set3}$ have a reduced number of operations when the Hydro is off.

Another reason affecting the quadrilateral characteristic with $I_{POL} = I_2$ is that when the fault resistance increases, the effective impedance measured by the relay presents an oscillatory behavior, as shown in Figure 8 for an AG fault with $Rf = 1.14\ \Omega, sec$ (i.e., 5 Ω in primary values). In this case, Potential Transformer Ratio (PTR) = 350 and Current Transformer Ratio (CTR) = 80. Due to fault resistance overestimation, a phenomenon caused by the fault resistance value and the magnitude of the short-circuit current contribution from the local and remote infeed [25], the relay would not detect the fault. However, in longer lines with an increased resistive reach, the relay may show an insecure behavior caused by the oscillations in the reactance reach.

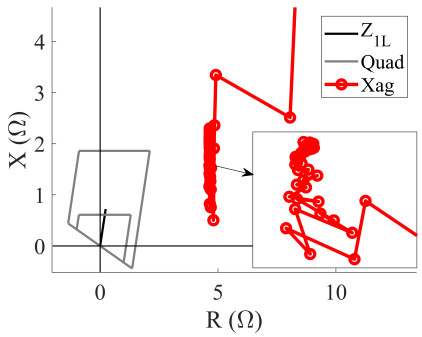

Fig. 8: Quadrilateral characteristic - AG fault, Rf = 1.14 $\Omega, sec.$

In addition, for lines fed by IBRs, there is no straightforward way to set the tilt angle for the reactance element using (4), since the local negative-sequence source impedance (i.e., Z_{2S}) for the IBR end is unpredictable and may vary during the fault. Moreover, such characteristics can cause additional errors in the effective impedance measurement, leading to unsecured behaviors.

The mho element response for ground faults was reliable. The only limitation is the inherent limited resistive reach in the element. Still, it covered more cases than the quadrilateral characteristic, as shown in Figure 7.

C. Sequence currents-based FID logic response

The FID logic is only effective if the power transformer behind the relay provides a zero-sequence current path and if the IBR regulates I_2 injection in compliance with IEEE Std. 2800-2022. Figure 9 presents the logic's response comparing the three different current controllers. A proper operation is achieved with positive and negative-sequence current control, see Figure 9a. Notice that the angle between I_0 and I_2 is within the region between -30 and 30 degrees, therefore, a phase-A-to-ground fault is correctly classified.

The FID logic response for the other current controllers did not classify any fault loops because the negative-sequence current level detector did not allow its operation. This current level detector monitors the magnitude of $|3I_2|$ against forward and reverse thresholds, $50FP$ and $50RP$, respectively. Figure 10 presents an example of an AG fault with the IBR controlling phase currents in the dq-domain. In this case, $|3I_2|$ is higher than the thresholds only for an initial transient period, which is not long enough for the logic to operate.

D. Ground Directional Elements

The conclusions for the ground directional elements are: the 32V element is reliable when a strong zero-sequence current path exists behind the relay. IBRs do not provide zero-sequence current to the grid. However, if a zero sequence path exists due to the ground in the power transformer, it allows zero-sequence current to circulate, and the 32V element to operate, as shown in Figure 11a. The 32QG element presents a proper fault signature with negative-sequence current control. However, this element is supervised by the zero-sequence restraining factor that monitors the ratio $|I_2|/|I_0|$ and compares against its threshold (i.e., $k_2 = 0.2$).

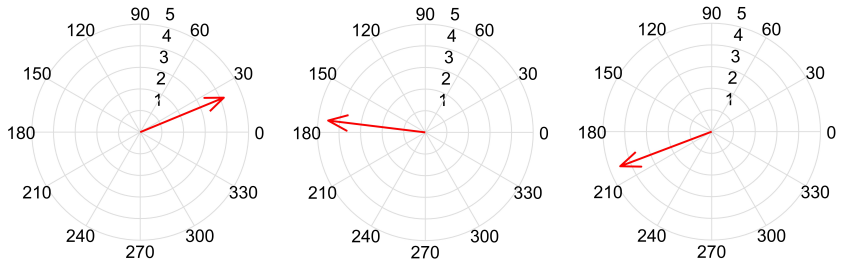

(a) Sequence currents-dq domain. (b) Phase currents-dq domain. (c) Phase currents-$\alpha\beta$ domain.

Fig. 9: FID logic response for different current controllers.

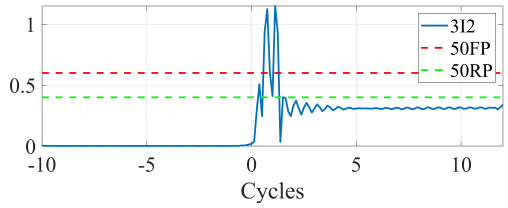

Fig. 10: $|3I_2|$ current level detector.

This ratio was below its threshold for all the cases and blocked the 32QG element operation, resulting in a 0% success rate. Figure 11b presents an example of the 32QG failing to operate.

E. Extra Analysis for Phase Faults

The analysis for phase distance elements performed in [12] proves that the quadrilateral characteristic highly depends on the IBR current controllers since the element is polarized using I_2. In addition, the mho characteristic for phase faults has abnormal expansion caused by the IBR current limiters. The mho circle exhibits large expansion and also rotates depending on whether the IBR provides active or reactive current during the fault (d-axis or q-axis priority). Figure 12 shows that the circle expands towards the imaginary axis if the inverter provides reactive current, whereas it expands towards the real axis if it provides active current. In both cases, the relay tripped. However, when the circle expands towards the real axis, it reduces fault resistance coverage since the circle rotation limits the resistive reach to the right of the R-X plan.

If the 32Q element supervises the phase distance elements, its operation relies on the negative-sequence current control. Figure 13 presents the 32Q element behavior comparing the phase currents control with the sequence current control, both in the dq-domain. The proper operation is obtained only for the cases with sequence current control for the IBR to supply negative sequence current with an appropriate phase angle relationship. In this case, $z2A < Z2FTH$ indicates a forward fault.

V. Conclusions

This work presented a sensitivity analysis for the operation of distance elements and their supervising functions considering different IBR current controllers under different

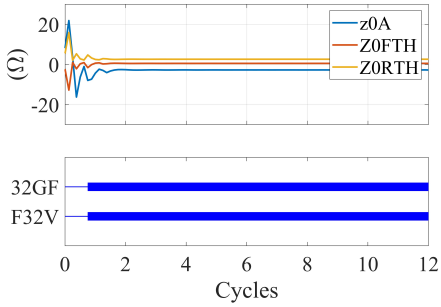

(a) 32V - F32V indicates forward fault.

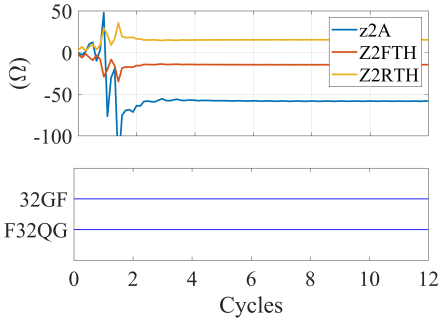

(b) 32QG - F32QG indicates forward fault..

Fig. 11: Ground directional elements operation.

fault conditions. The protection elements that have a reliable response for the cases evaluated here include the I_0 polarized quadrilateral element for ground faults, the 32V directional element, and the memory polarized mho element for ground faults. Elements that rely on the negative-sequence current behavior have an improved operation when the current controllers from the inverters meet compliance with IEEE Std. 2800-2022. The mho phase distance elements have abnormal circle expansion because of current limiters, and their resistive coverage is reduced when the circle expands towards the real axis. Recent research directions point to developing or using protection elements that are agnostic to sources feeding the fault. In addition, commercial relays have alternatives to improve protection security.

It includes using self-polarized quadrilateral elements for phase faults, but they come with the cost of being impacted

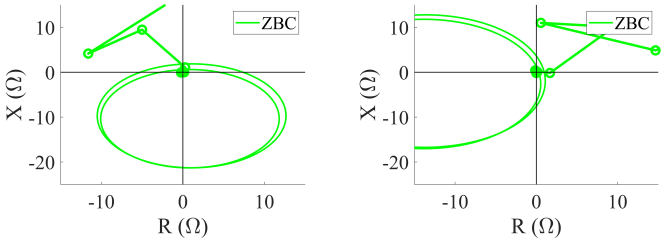

(a) Q axis priority. (b) D axis priority.

Fig. 12: Mho phase element for different current priorities.

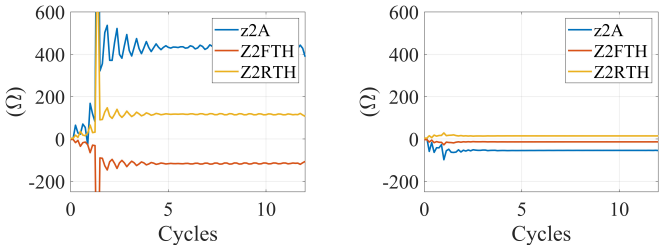

(a) Phase currents - dq-domain. (b) Sequence currents - dq domain.

Fig. 13: 32Q element behavior for different current controllers.

by load-flow conditions. The offset mho distance element can be an alternative to the memory-polarized one for phase and ground faults. Undervoltage-based FID is presented as an alternative to the sequence currents FID logic [26]. Despite these alternative recommendations, sensitivity analysis of these elements is still needed to prove their security. This task is included as the next step of this research.

REFERENCES

[1] U. Muenz, S. Bhela, N. Xue, A. Banerjee, M. J. Reno, D. Kelly, E. Farantatos, A. Haddadi, D. Ramasubramanian, and A. Banaie, "Protection of 100 % Inverter-dominated Power Systems with Grid-Forming Inverters and Protection Relays - Gap Analysis and Expert Interviews," Sandia National Laboratories, Albuquerque, Tech. Rep. April, 2024.

[2] F. V. Lopes, M. J. B. B. Davi, M. Oleskovicz, A. Hooshyar, X. Dong, and A. A. A. Neto, "Maturity Analysis of Protection Solutions for Power Systems Near Inverter-Based Resources," *IEEE Transactions on Power Delivery*, vol. 39, no. 5, pp. 2630–2643, 10 2024. [Online]. Available: https://ieeexplore.ieee.org/document/10577496/

[3] M. Nagpal and C. Henville, "Impact of Power-Electronic Sources on Transmission Line Ground Fault Protection," *IEEE Transactions on Power Delivery*, vol. 33, no. 1, pp. 62–70, 2 2018. [Online]. Available: http://ieeexplore.ieee.org/document/7935410/

[4] S. Chakraborty, P. H. Pinheiro, G. B. Romulo, H. Lei, B. K. Johnson, S. Manson, J. Wang, R. Mahmud, A. Hoke, and C. J. Kruse, "Studying the Impact of IBR Modeling on the Commonly Applied Transmission Line Protective Elements," in *IEEE Energy Conversion Congress & Expo*. Phoenix: IEEE, 2024, pp. 1–9.

[5] P. Adhikari, S. Brahma, and P. H. Gadde, "Source-Agnostic Time-Domain Distance Relay," *IEEE Transactions on Power Delivery*, vol. 37, no. 5, pp. 3620–3629, 10 2022. [Online]. Available: https://ieeexplore.ieee.org/document/9640501/

[6] P. Adhikari and S. Brahma, "Source-Agnostic Time-Domain Directional Relay," *IEEE Transactions on Power Delivery*, vol. 39, no. 2, pp. 1247–1258, 2024.

[7] E. O. Schweitzer III, M. V. Mynam, D. E. Whitehead, B. Z. Kastenny, A. Guzman-Casillas, and V. Skendzic, "US Patent No 10,310,005 B2 - Time-Domain Distance Line Protection of Electric Power Delivery Systems," 2019.

[8] E. O. S. III, M. V. Mynam, D. E. Whitehead, B. Z. Kastenny, A. Guzman-Casillas, and V. Skendzic, "US Patent No. 10,310,004 B2 -Time-Domain Differential Line Protection of Electric Power Delivery Systems," 2019.

[9] O. D. Naidu, N. George, S. Zubic, and M. Krakowski, "Time-Domain-Based Distance Protection for Transmission Networks: Secure and Reliable Solution for Complex Networks," *IEEE Access*, vol. 11, no. September, pp. 104 656–104 675, 2023. [Online]. Available: https://ieeexplore.ieee.org/document/10252060/

[10] IEEE Power and Energy Society, "IEEE Standard for Interconnection and Interoperability of Inverter-Based Resources (IBRs) Interconnecting with Associated Transmission Electric Power Systems," Piscataway, NJ, USA, pp. 1–177, 2 2022. [Online]. Available: https://ieeexplore.ieee.org/document/9762253/

[11] M. J. Davi, M. Oleskovicz, and F. V. Lopes, "Study on IEEE 2800-2022 Standard Benefits for Transmission Line Protection in the Presence of Inverter-Based Resources," *Electric Power Systems Research*, vol. 220, no. February, p. 109304, 7 2023. [Online]. Available: https://doi.org/10.1016/j.epsr.2023.109304 https://linkinghub.elsevier.com/retrieve/pii/S0378779623001931

[12] P. Pinheiro, S. Chakraborty, R. Bainy, H. Lei, B. K. Johnson, A. Alomari, S. Manson, J. Wang, R. Mahmud, A. Hoke, and C. J. Cruse, "Benefits and Recommendations for Using Classic Protection Functions in Transmission Lines Interfacing IBRs Compliant to IEEE 2800," in *2024 Grid of the Future Symposium*. Raleigh: CIGRE, 2024, pp. 1–12.

[13] R. Teodorescu, M. Liserre, and P. Rodríguez, *Grid Converters for Photovoltaic and Wind Power Systems*. Wiley, 1 2011. [Online]. Available: https://onlinelibrary.wiley.com/doi/book/10.1002/9780470667057

[14] B. Fan, T. Liu, F. Zhao, H. Wu, and X. Wang, "A Review of Current-Limiting Control of Grid-Forming Inverters under Symmetrical Disturbances," *IEEE Open Journal of Power Electronics*, vol. 3, no. October, pp. 955–969, 2022.

[15] D. Hou, A. Guzman, and J. Roberts, "Innovative Solutions Improve Transmission Line Protection," in *24th Annual Western Protective Relay Conference*. Spokane: SEL, 1997, pp. 1–25.

[16] E. O. I. Schweitzer, "New Developments in Distance Relay Polarization and Fault Type Selection," in *16th Annual Western Protective Relay Conference, Spokane, WA*, no. October 1989. Spokane: SEL, 1991, p. 18.

[17] Schweitzer Engineering Laboratories Inc., "SEL-411L Relay Instruction Manual Advanced Line Differential Protection, Automation, and Control System," Pullman, 2016.

[18] E. O. Schweitzer III and J. Roberts, "Distance Relay Element Design," *SEL Journal of Reliable Power*, vol. 1, no. 1, pp. 1–26, 2010.

[19] A. Banaiemoqadam, A. Azizi, A. Hooshyar, and E. F. El-Saadany, "Impact of Inverter-Based Resources on Different Implementation Methods for Distance Relays - Part II: Reactance Method," *IEEE Transactions on Power Delivery*, vol. 38, no. 6, pp. 4049–4060, 2023.

[20] K. Dase, A. Guzmán, S. Chase, and B. Smyth, "Applying Dependable and Secure Protection With Quadrilateral Distance Elements," in *Georgia Tech Protective Relaying Conference*. Atlanta: SEL, 2023, pp. 1–19.

[21] S. E. Zocholl, "Three-Phase Circuit Analysis and the Mysterious k0 Factor," *22nd Annual Western Protective Relay Conference Spokane, Washington*, no. April, pp. 0–17, 1995.

[22] H. J. A. Ferrer and E. O. S. III, *Modern Solutions for Protection, Control, and Monitoring of Electric Power Systems*, 1st ed. Pullman: SEL, 2010.

[23] A. Guzmán, J. Roberts, and D. Hou, "New Ground Directional Elements Operate Reliably for Changing System Conditions," in *Beijing Electric Power International Conference on Transmission and Distribution*, no. November. Beijing: SEL, 1997.

[24] D. Costello and K. Zimmerman, "Determining the Faulted Phase," in *36th Annual Western Protective Relay Conference*. Spokane: SEL, 2009, pp. 1–20.

[25] Y. Liang, Z. Lu, W. Li, W. Zha, and Y. Huo, "A Novel fault impedance calculation method for distance protection against fault resistance," *IEEE Transactions on Power Delivery*, vol. 35, no. 1, pp. 396–407, 2020.

[26] R. McDaniel, R. Chowdhury, K. Zimmerman, and B. Cockerham, "Applying SEL Relays In Systems With Inverter-Based Resources," Pullman, pp. 1–26, 2021.